IJMMM
International Journal of
Minerals, Metallurgy and Materials
矿物冶金与材料学报（英文版）

Experimental and *ab initio* study of $Ba_2Na_3(B_3O_6)_2F$ stability in the pressure range of 0–10 GPa

Nursultan E. Sagatov, Tatyana B. Bekker, Yulia G. Vinogradova, Alexey V. Davydov, Ivan V. Podborodnikov, and Konstantin D. Litasov

Cite this article as:

Nursultan E. Sagatov, Tatyana B. Bekker, Yulia G. Vinogradova, Alexey V. Davydov, Ivan V. Podborodnikov, and Konstantin D. Litasov, Experimental and *ab initio* study of $Ba_2Na_3(B_3O_6)_2F$ stability in the pressure range of 0–10 GPa, *Int. J. Miner. Metall. Mater.*, 30(2023), No. 9, pp. 1846-1854. https://doi.org/10.1007/s12613-023-2647-0

International Journal of Minerals, Metallurgy and Materials
Volume 30, Number 9, September 2023, Page 1846
https://doi.org/10.1007/s12613-023-2647-0

Experimental and *ab initio* study of $Ba_2Na_3(B_3O_6)_2F$ stability in the pressure range of 0–10 GPa

Nursultan E. Sagatov[1,2),✉], *Tatyana B. Bekker*[1,2,3)], *Yulia G. Vinogradova*[1,2)], *Alexey V. Davydov*[1,2)], *Ivan V. Podborodnikov*[1,2)], *and Konstantin D. Litasov*[4,5)]

1) Sobolev Institute of Geology and Mineralogy, Siberian Branch of Russian Academy of Sciences, Novosibirsk 630090, Russia
2) Department of Geology and Geophysics, Novosibirsk State University, Novosibirsk 630090, Russia
3) Research and Development Department, Novosibirsk State University of Architecture, Design and Arts (NSUADA), Novosibirsk 630099, Russia
4) Vereshchagin Institute for High Pressure Physics, Russian Academy of Sciences, Troitsk 108840, Russia
5) Fersman Mineralogical Museum, Russian Academy of Sciences, Moscow 119071, Russia

(Received: 9 December 2022; revised: 3 April 2023; accepted: 7 April 2023)

Abstract: Both numerical and experimental studies of the stability and electronic properties of barium–sodium metaborate $Ba_2Na_3(B_3O_6)_2F$ ($P6_3/m$) at pressures up to 10 GPa have been carried out. Electronic-structure calculations with HSE06 hybrid functional showed that $Ba_2Na_3(B_3O_6)_2F$ has an indirect band gap of 6.289 eV. A numerical study revealed the decomposition of $Ba_2Na_3(B_3O_6)_2F$ into the BaB_2O_4, $NaBO_2$, and NaF phases above 3.4 GPa at 300 K. Subsequent high-pressure high-temperature experiments performed using 'Discoverer-1500' DIA-type apparatus at pressures of 3 and 6 GPa and temperature of 1173 K confirmed the stability of $Ba_2Na_3(B_3O_6)_2F$ at 3 GPa and its decomposition into BaB_2O_4, $NaBO_2$, and NaF at 6 GPa, which was verified by energy-dispersive X-ray analysis and Raman spectroscopy. The observed Raman bands of the $Ba_2Na_3(B_3O_6)_2F$ phase were assigned by comparing the experimental and calculated spectra. The experimental Raman spectra of decomposition reaction products obtained at 6 GPa suggest the origin of a new high-pressure modification of barium metaborate BaB_2O_4.

Keywords: density functional theory; phase stability; borate; high pressure; Raman spectroscopy

1. Introduction

Barium–sodium metaborate $Ba_2Na_3(B_3O_6)_2F$ ($P6_3/m$) found as a reaction product in the BaB_2O_4–NaF system [1] is known for its prominent birefringent properties both in the ultraviolet [2–4] and terahertz regions [5]. It belongs to the so-called metaborates as its main structural element is an isolated metaboric ring, $[B_3O_6]^{3-}$, consisting of three $[BO_3]^{3-}$ triangles linked via three bridging oxygen atoms. Known metaborates, which are the salts of the low-temperature modification of metaboric acid α-HBO_2 ($Pbnm$), include alkaline metals salts with structural formula $M_3[BO_2]_3$ (M = Na, K, Rb, Cs) ($R\bar{3}c$) [6–9], alkaline-earth and transition metals salts such as α-BaB_2O_4 ($R\bar{3}c$) [10], β-BaB_2O_4 ($R3c$) [11], and $Ba_2M(B_3O_6)_2$ (M = Ca, Cd, Mg, Co, Ni) ($R\bar{3}$) [12]. The structure of barium–sodium metaborate $Ba_2Na_3(B_3O_6)_2F$ is similar to the structure of a high-temperature modification of barium metaborate α-BaB_2O_4: both structures have pseudolayered arrangement of metaboric rings perpendicular to the *c* axis, with the difference that in the structure of $Ba_2Na_3(B_3O_6)_2F$ six-coordinated barium atoms are replaced by $[Na_3F]^{2+}$ groups according to the scheme $Ba^{2+} \rightarrow [Na_3F]^{2+}$ [4].

The effect of high pressure on the crystal structure and properties of borates has been an actively developing area of research for many years [13–15]. The study of high-pressure borates aids in the understanding of both their crystal-chemical regularities as well as their potential to create new functional materials. Our recent attempt to assess the stability of the BaB_2O_4 compound at pressures up to 10 GPa using first-principles calculations [16] in conjunction with subsequent experiment at a pressure of 3 GPa led to the discovery of γ-BaB_2O_4 ($P2_1/n$) modification [17]. The central role in its structure is played by edge-sharing BO_4 tetrahedra, first described in the $Dy_4B_6O_{15}$ compound by Huppertz and von der Eltz [18].

In this paper, we address the electronic properties of the $Ba_2Na_3(B_3O_6)_2F$ compound, establish a connection between the structure and Raman scattering based on the comparison of experimental and calculated spectra, and provide the evidence for $Ba_2Na_3(B_3O_6)_2F$ high-pressure decomposition into sodium fluoride, sodium borate, $NaBO_2$, and new high-pressure modification of barium borate, δ-BaB_2O_4.

✉ Corresponding author: Nursultan E. Sagatov E-mail: sagatinho23@gmail.com

2. Computational and experimental details

2.1. Computational methods

All calculations were performed within the density functional theory (DFT) implemented in the VASP 5.4.4 [19–20]. The exchange–correlation interaction was taken into account in the generalized gradient approximation in the form of the Perdew–Burke–Ernzerhof (PBE) functional [21]. The electron–ion interaction was described by applying the projector–augmented–wave (PAW) method with the following valence electron configurations of atoms: $5s^2 5p^6 6s^2$ for Ba, $3s^1 3p^0$ for Na, $2s^2 2p^1$ for B, $2s^2 2p^4$ for O, and $2s^2 2p^5$ for F. The total energies of the structures were minimized by relaxing the structural parameters and atomic coordinates at different pressures using a conjugated gradient optimization method. The relaxation of the structure was performed with maximum tolerances for the energy of 1.0×10^{-7} eV and stress of 0.01 GPa. Forces between atoms are minimized down to 0.001 eV/Å. The energy cutoff was set to 700 eV. By adopting the Γ-centered Monkhorst-Pack method [22], the Brillouin zone was sampled with a k-mesh density of $2\pi \times 0.03$ Å^{-1}. Electron smearing was employed using the Gaussian-smearing technique with smearing parameter $\sigma = 0.05$ eV. The elastic constants C_{ij} were calculated from the stress (σ)–strain (ε) relation $\sigma_i = C_{ij} \times \varepsilon_j$, where $i, j = 1$–6. Since the use of the PBE functional tends to severely underestimate the width of the band gap, the HSE06 hybrid functional [23] was used to calculate the density of states (DOS) and band structure of $Ba_2Na_3(B_3O_6)_2F$. A high-symmetry path for the calculation of electronic band structure was generated by the VASPKIT tool [24]. It is worth nothing that hybrid DFT is limited by tradeoffs between over-delocalization and under-binding, and thus, it can still underestimate width of the band gaps. There are some approaches, such as self-interaction corrections, localized orbital scaling corrections, and rung-3.5, that can help mitigate these tradeoffs' impact the electronic structure [25–27].

To calculate the phonon spectra and pressure–temperature (P–T) phase diagram, the PHONOPY [28] program was exploited. The temperature effect was considered within the quasiharmonic approximation (QHA). Real-space force constants were calculated using supercell and finite-displacement approaches with a $2 \times 2 \times 1$ supercell.

The Raman spectra were obtained using *vasp_raman.py* code [29] by calculating the dielectric tensors for each vibrational mode. To match the experimental spectrum, the calculated Raman spectrum was calibrated using a scaling factor, which is the ratio of Raman shifts of the most intensive peaks in experimental and calculated Raman spectra. In the present study, the scaling factor was 1.033. The animations and visualization of Raman active vibrations were made by VaspVib2XSF [30], PHONOPY [28], and OVITO tools [31].

2.2. Experimental techniques

2.2.1. High-pressure high-temperature synthesis

The synthesis of β-BaB_4O_7 was carried out on the 'Discoverer-1500' DIA-type apparatus at the Sobolev Institute of Geology and Mineralogy SB RAS in Novosibirsk, Russia. The design and characteristics of the high-pressure cell used in this work were described in detail in Ref. [17].

As initial samples for high-pressure high-temperature (HPHT) experiments we used grounded $Ba_2Na_3(B_3O_6)_2F$ crystal, grown in the BaB_2O_4–NaF system [1], and the polycrystalline sample obtained by solid phase synthesis (SPS) according to reaction (1):

$$\begin{aligned}&2BaCO_3 + NaF + Na_2CO_3 + 6HBO_2 \rightarrow \\ &\quad Ba_2Na_3(B_3O_6)_2F + 3CO_2\uparrow + 3H_2O\uparrow\end{aligned} \qquad (1)$$

The samples were placed in a graphite cassette with holes of 0.9 mm in diameter and 1.1 mm deep. Experiments were carried out by compressing to 3 MN and 6 MN (corresponding to a pressure of 3 GPa and 6 GPa, respectively), and heating to the temperature of 1173 K at a rate of 100 K/min. The heating was stopped by switching off the voltage supplied to the heater. The maximum temperature gradient in the working volume with samples is estimated at 4–5 K/mm at 1073 K. Accordingly, in the working volume of the sample we distinguish high (HT) and low (LT) temperature zones. The temperature drop rate was about 100 K/s. Decompression to ambient-pressure conditions took 180 min. The duration of the experiment at 3 GPa, 1173 K was 44.5 h, and at 6 GPa, 1173 K was 64 h.

2.2.2. Scanning electron microscopy

Annealed samples were studied using a MIRA 3 LMU scanning electron microscope (Tescan Orsay Holding, Brno-Kohoutovice, Czech Republic) coupled with an INCA energy-dispersive X-ray microanalysis system 450 equipped with the liquid nitrogen-free Large area EDS X-Max-80 Silicon Drift Detector (Oxford Instruments Nanoanalysis Ltd., High Wycombe, UK) at IGM SB RAS.

2.2.3. Raman spectroscopy

The Raman spectra were recorded on a Horiba Jobin Yvon LabRAM HR800 (France) spectrometer with 1024 pixel LN/CCD detector using the 532 nm wavelength (tunable Ar^+ laser) in IGM SB RAS and collected in a backscattering geometry using Olympus BX41 confocal microscope. The spectral resolution of the recorded Stokes side of the Raman spectrum was set to ~2.0 cm^{-1} at a Raman shift of 1300 cm^{-1}.

3. Results and discussion

3.1. Structure stability and electronic properties

The stability of the $Ba_2Na_3(B_3O_6)_2F$ compound in the pressure range of 0–10 GPa has been considered relative to two possible reactions of decomposition:

$$Ba_2Na_3(B_3O_6)_2F \leftrightarrow 2BaB_2O_4 + 2NaBO_2 + NaF \qquad (2)$$

$$Ba_2Na_3(B_3O_6)_2F \leftrightarrow 3/2BaB_2O_4 + 3NaBO_2 + 1/2BaF_2 \qquad (3)$$

For the calculations, the structures of known polymorphs of BaB_2O_4 ($\beta \xrightarrow{0.8\text{ GPa}} \gamma \xrightarrow{6.8\text{ GPa}} Pa\bar{3}$) [17] and BaF_2 ($Fm\bar{3}m \xrightarrow{3.5\text{ GPa}} Pnma$) [16,32] were taken into account. NaF and $NaBO_2$ were considered in the form of $Fm\bar{3}m$ [33] and $R\bar{3}c$ [34] structures, respectively, in the entire considered pressure range.

Fig. 1 depicts enthalpy–pressure dependencies calculated without taking into account zero-point energy (ZPE). It can be seen that the decomposition of $Ba_2Na_3(B_3O_6)_2F$ in accordance with reaction (2) occurs at a pressure of 2.8 GPa. Reaction (3) is energetically unfavorable relative to reaction (2) over the entire pressure range. This result suggests that above 2.8 GPa $Ba_2Na_3(B_3O_6)_2F$ should decompose to $2BaB_2O_4$ + $2NaBO_2$ + NaF.

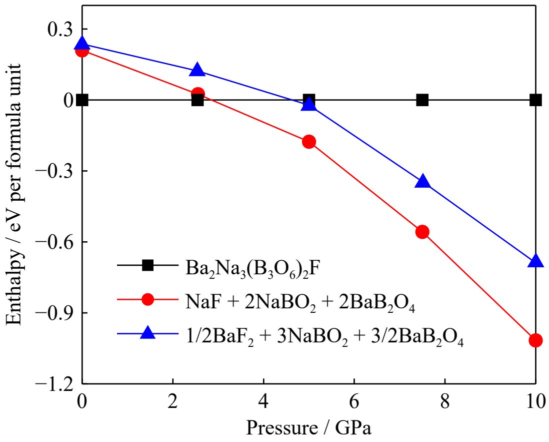

Fig. 1. Relative enthalpy–pressure dependencies of $Ba_2Na_3(B_3O_6)_2F$ and two isochemical mixtures.

To estimate the mechanical stability of $Ba_2Na_3(B_3O_6)_2F$, the elastic constants C_{ij} were calculated (Table S1) and then the Born stability criteria were applied. The Born stability criteria form a set of necessary and sufficient conditions that determine whether a given material is stable. For hexagonal crystal under a hydrostatic pressure P, there are three Born stability criteria [35]:

$$C_{11} - C_{12} - 2P > 0,$$

$$(C_{11} + 2C_{12} + P)(C_{33} - P) - 2(C_{13} + P)^2 > 0,$$

$$C_{44} - P > 0.$$

In our case, the first and second stability criteria are satisfied in the entire considered pressure range. The third stability criterion is met up to ~5 GPa (Fig. 2). Above this pressure, the value of $(C_{44} - P)$ becomes negative (Fig. 2) which indicate the mechanical instablity of $Ba_2Na_3(B_3O_6)_2F$ above 5 GPa.

To assess the dynamic stability and the effect of temperature on the decomposition pressure of $Ba_2Na_3(B_3O_6)_2F$, phonon spectra were calculated at various pressures. The absence of imaginary modes in phonon spectra indicates that $Ba_2Na_3(B_3O_6)_2F$ is dynamically stable at 0–5 GPa (Fig. 3), which lends support to the use of QHA in this pressure range. Above 5 GPa, imaginary modes appear, indicating dynamic instability. In addition, the absence of imaginary modes and meeting Born stability criteria imply that $Ba_2Na_3(B_3O_6)_2F$ can be metastably compressed without heating up to 5 GPa.

Based on the calculations of Gibbs free energy at different temperatures, P–T diagram of $Ba_2Na_3(B_3O_6)_2F$ was constructed (Fig. 4). The consideration of ZPE increases the decomposition pressure from 2.8 to 3.1 GPa at zero temperature. According to the obtained results, at 300 K the decomposition of $Ba_2Na_3(B_3O_6)_2F$ occurs at 3.4 GPa with a positive Clapeyron slope of 0.9 MPa/K. It should be noted that constructed P–T diagram is valid in case of the absence of phase transitions of $Ba_2Na_3(B_3O_6)_2F$.

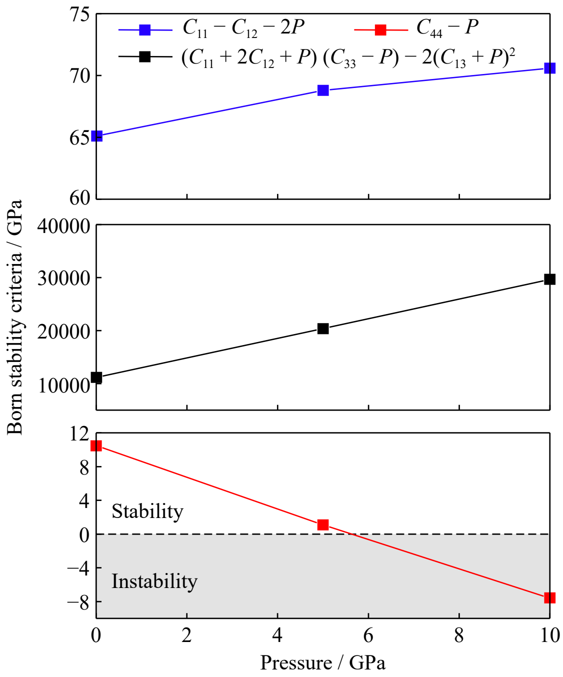

Fig. 2. Born stability criteria as a function of the applied pressure.

According to the band-structure calculation, $Ba_2Na_3(B_3O_6)_2F$ is an insulator with an indirect band gap (E_g) of 6.289 eV along the Γ–K direction (Fig. 5(a)). The obtained value of the band gap is in good agreement with the experimentally obtained UV transmittance cut-off edge, which is located according to different studies at about 200 nm (6.20 eV) [1], 186 nm (6.66 eV) [2] and 175 nm (7.08 eV) [3].

The calculation of the density of states (Fig. 5(b)) shows that the bottom of the valence band is composed of occupied Ba 5p states (about −10 eV). The band centered at −8.3 eV is formed by O 2p and B 2s states, and the bands from −7.6 to −2.7 eV are formed by O 2p and B 2p states. This implies that O 2p orbitals are hybridized with the B 2s and 2p orbitals. It is worth noting that the contributions of B 2s and 2p states are smaller than the contribution of O 2p states. The valance band region from −2.6 eV to −2.0 eV is contributed by O 2p states and F 2p states. In the upper part of the valence band above −2.0 eV, the O 2p states make the main contribution. The conduction band consists of unoccupied Ba 5d states with a small contribution from unoccupied B 2p, O 2p, and Na 3s states. These results indicate that the main optical transition occurs from O 2p orbitals to Ba 5d levels with a change in the orbital angular momentum $\Delta l = 1$. Such transitions generally are characteristic of barium borates [17,36–38].

3.2. Raman spectroscopy of $Ba_2Na_3(B_3O_6)_2F$

Since the number of experimental methods suitable for studying HPHT synthesis products is limited by the small

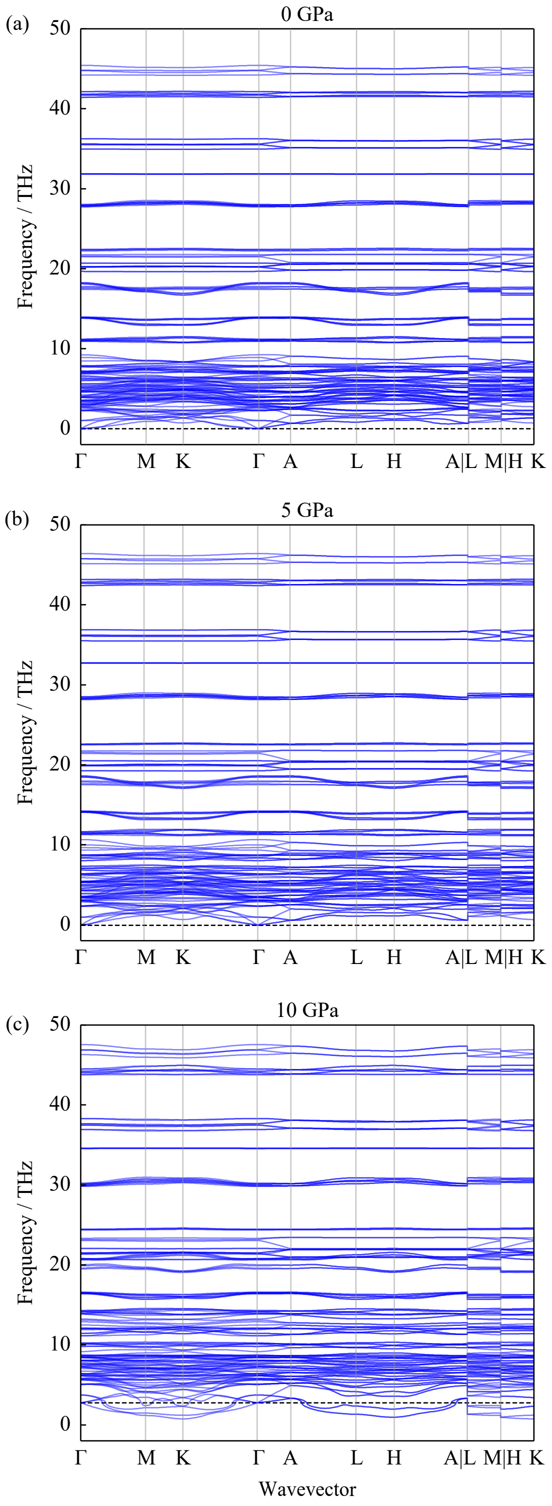

Fig. 3. Calculated phonon spectra of $Ba_2Na_3(B_3O_6)_2F$ at (a) 0, (b) 5, and (c) 10 GPa.

size of the samples, Raman spectroscopy has gained increasing prominence for the identification of polymorphs.

From the group analysis of $Ba_2Na_3(B_3O_6)_2F$, the optical modes at the Γ point belong to the following irreducible representations: $\Gamma_{optical} = 12A_g + 11A_u + 12B_g + 12B_u + 11E_{1g} + 12E_{1u} + 13E_{2g} + 11E_{2u}$, where 36 modes, $\Gamma_{Raman} = 12A_g + 13E_{2g} + 11E_{1g}$, are Raman-active modes. Fig. 6 and Table 1 show the experimental Raman spectra of $Ba_2Na_3(B_3O_6)_2F$ synthesized at ambient pressure in comparison with the results of DFT calculation in the range from 50 to 1700 cm^{-1}. All calculated Raman shifts are close to the experimental value.

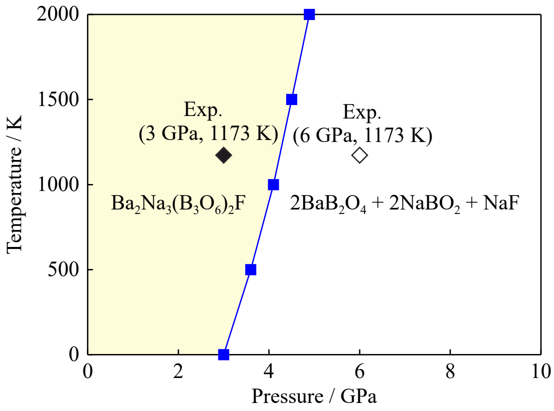

Fig. 4. *P–T* phase diagram of $Ba_2Na_3(B_3O_6)_2F$.

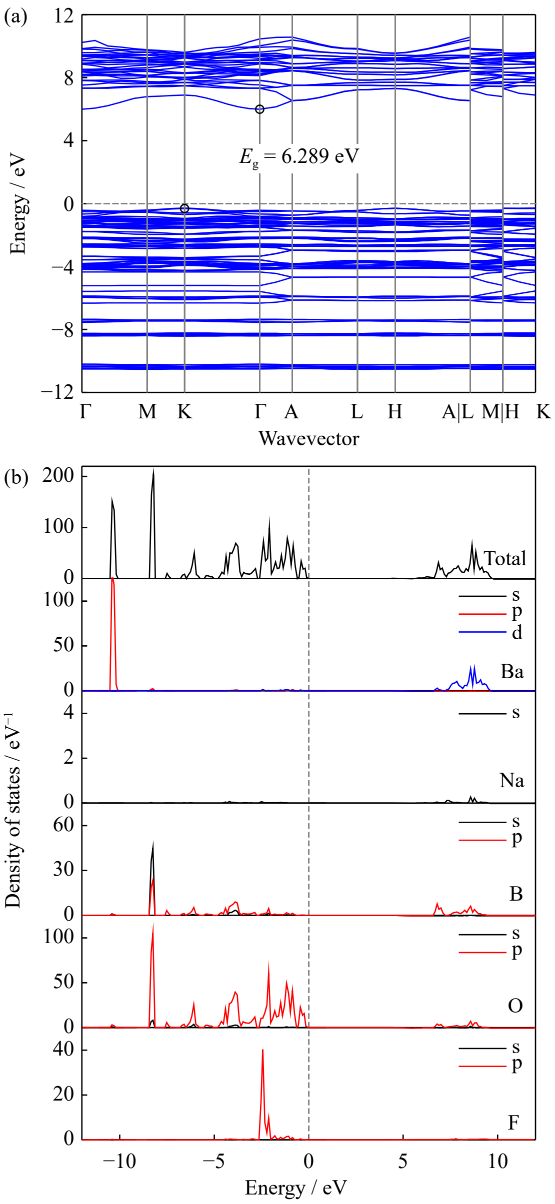

Fig. 5. Calculated (a) band structure and (b) total and partial DOS of $Ba_2Na_3(B_3O_6)_2F$.

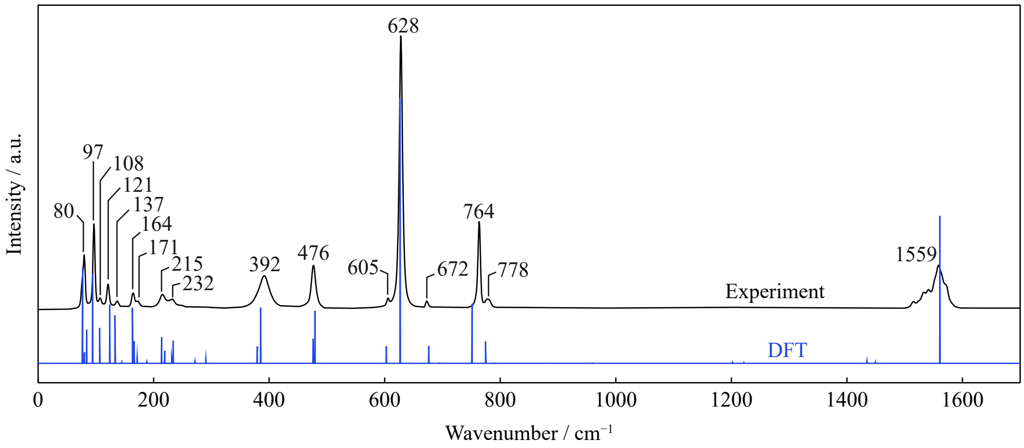

Fig. 6. Experimental and calculated (DFT) unoriented Raman spectra of $Ba_2Na_3(B_3O_6)_2F$.

Table 1. Experimental and calculated Raman active modes of $Ba_2Na_3(B_3O_6)_2F$

Observed / cm^{-1}	Calculated / cm^{-1}	Mulliken symbol	Observed / cm^{-1}	Calculated / cm^{-1}	Mulliken symbol
1559	1561	A_g	215	214	E_{2g}
778	771	A_g	171	171	E_{2g}
764	748	A_g	164	163	A_g
672	676	E_{1g}	137	133	A_g
628	628	A_g	120	124	E_{1g}
605	602	A_g	108	107	E_{2g}
476	479	E_{2g}	97	95	E_{2g}
392	385	E_{2g}	80	77	E_{1g}
232	235	E_{1g}	—	—	—

Generally, in metaborates peaks below ~300 cm^{-1} are attributed to the external modes of the crystal, while the peaks above ~300 cm^{-1} are attributed to the internal vibrational modes of $(B_3O_6)^{3-}$ rings [39]. The Raman peak at about 1559 cm^{-1} arises from the symmetric stretching vibration of B–O bonds (Fig. 7(a)). In the experimental spectrum, it splits into several peaks (Fig. 6). In $Ba_2Mg(B_3O_6)_2$ the splitting of the peak at about 1525 cm^{-1} related to the stretching vibration of B–O bonds into four peaks, is accounted for by an isotopic effect [40]. The peak at 764 cm^{-1} is associated with bending vibrations of B–O bonds (Fig. 7(b)). The strongest Raman mode in the spectra of all studied metaborates is accounted for by the breathing vibration of $(B_3O_6)^{3-}$ ring. Its position is believed to be insensitive to the surrounding atoms, which is confirmed by several experimental studies [39–41]. In $Ba_2Na_3(B_3O_6)_2F$, the breathing vibration is observed at 628 cm^{-1} (Fig. 7(c)). The modes at 476 cm^{-1} (Fig. 7(d)) and 392 cm^{-1} (Fig. 7(e)) are attributed to the mixed bending and libration vibration of $(B_3O_6)^{3-}$, while at 392 cm^{-1} vibrations of F^- and Na^+ are also attending. The Raman shifts below 232 cm^{-1} are related to mixed libration and translation vibrations of the $(B_3O_6)^{3-}$ ring together with translations of F^-, Na^+, and Ba^{2+} ions (Fig. 7(f)–(i)).

3.3. Study of the products of high-pressure high-temperature synthesis

Here we would like to draw attention to the results of two HPHT experiments conducted at a temperature of 1173 K and pressure of 3 GPa and 6 GPa, respectively (Fig. 8, Table 2). In both experiments grounded $Ba_2Na_3(B_3O_6)_2F$ crystal and synthesized $Ba_2Na_3(B_3O_6)_2F$ were used as starting materials.

At 3 GPa, a single-phase sample with a composition close to $Ba_2Na_3(B_3O_6)_2F$ was observed for the grounded crystal (Fig. 8(a)), while for the synthesized starting material small inclusions of the second phase, BaB_2O_4, were also present (Fig. 8(b) and (c)). We put emphasis on the fact that the Raman spectrum of $Ba_2Na_3(B_3O_6)_2F$ phase at 3 GPa coincided with the spectrum at atmospheric pressure which suggests that no phase transition occurs (Fig. 9(a) and (b)).

In contrast to the results of the experiment at 3 GPa, we have not found $Ba_2Na_3(B_3O_6)_2F$ in the reaction products of the experiment at 6 GPa. Based on the results of energy-dispersive X-ray microanalysis, the phases formed at 6 GPa are BaB_2O_4, $NaBO_2$, and NaF, which lends support to the correctness of the calculated P–T diagram (Fig. 4). It is worth noting that the size of BaB_2O_4 crystals formed is very small and does not exceed several microns (Fig. 8(d)–(f)). The most intriguing results have been revealed with the use of Raman scattering. As the NaF compound, being an ionic one, provides a very weak or no Raman signal, the observed Raman peaks might belong to $NaBO_2$ and BaB_2O_4 compounds (Fig. 9(c) and (d)). Fig. S1 shows the Raman spectrum of the reaction products at 6 GPa in comparison with the Raman spectra of the $NaBO_2$ ($R\bar{3}c$) phase [42]. Based on the comparison, we can draw the conclusion that peaks at about 126,

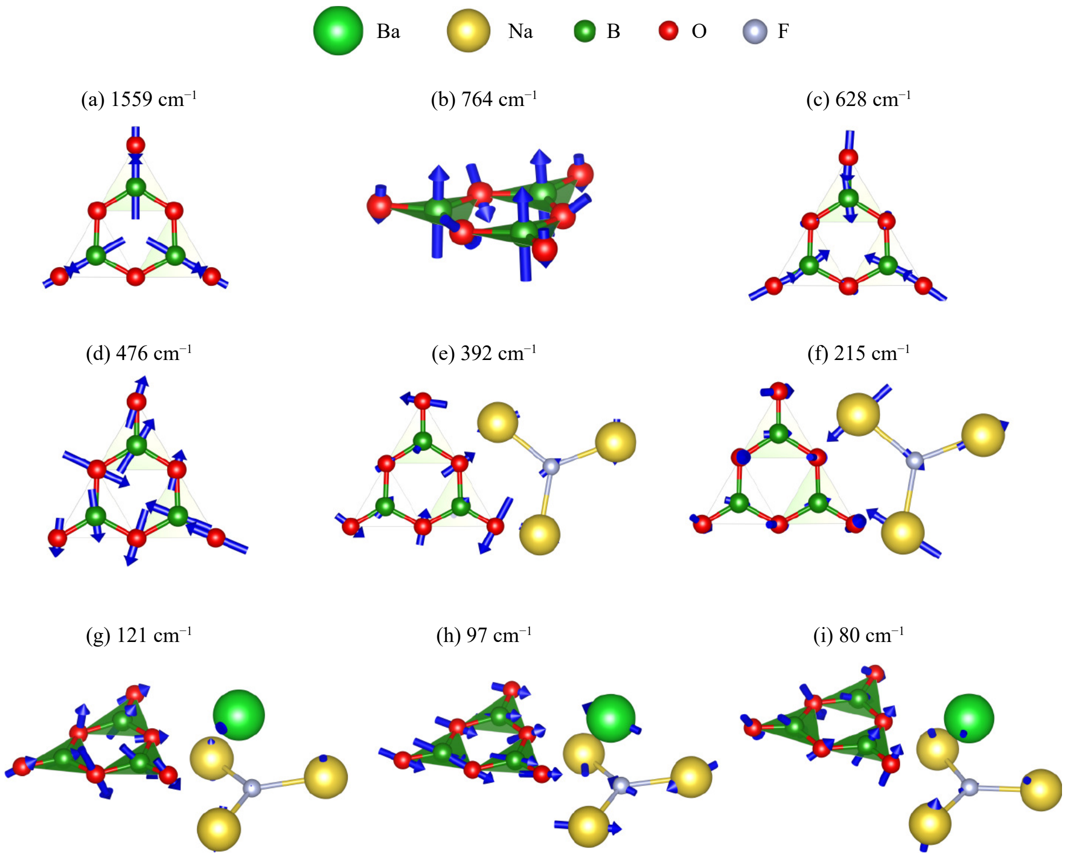

Fig. 7. Atom displacements in selected Raman modes of $Ba_2Na_3(B_3O_6)_2F$ at (a) 1559 cm^{-1}, (b) 764 cm^{-1}, (c) 628 cm^{-1}, (d) 476 cm^{-1}, (e) 392 cm^{-1}, (f) 215 cm^{-1}, (g) 121 cm^{-1}, (h) 97 cm^{-1}, and (i) 80 cm^{-1}. Arrows represent displacement vectors. Animated harmonic modes are available in the *Supporting Information*.

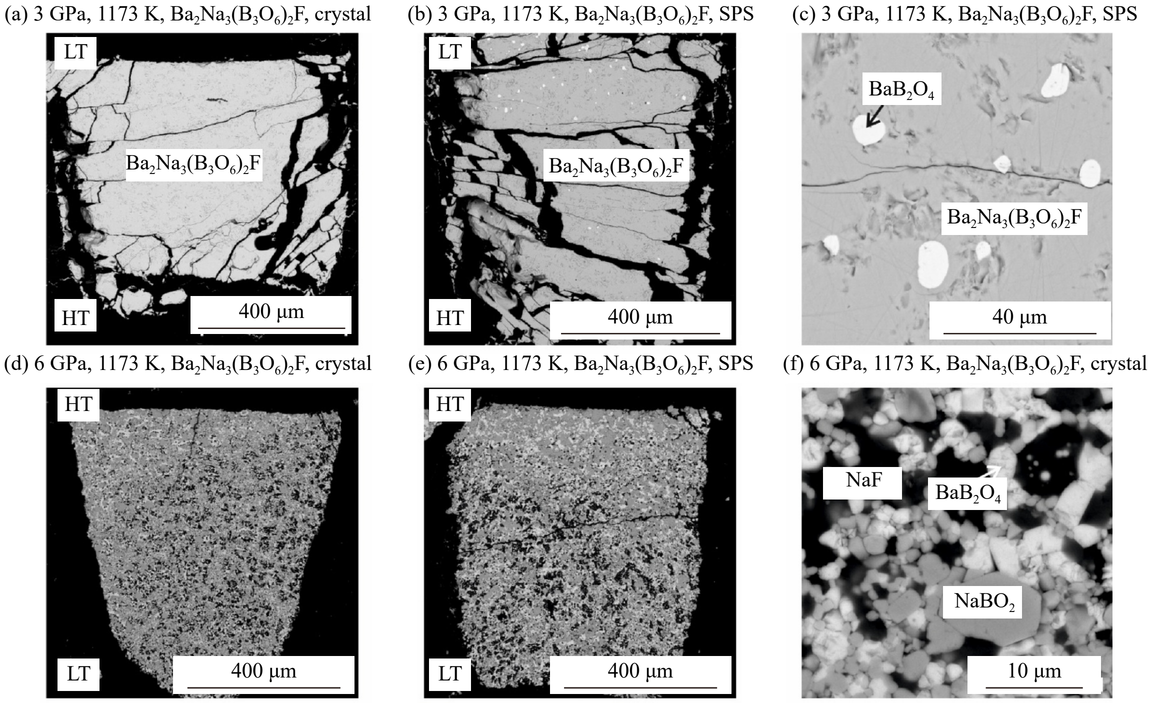
(a) 3 GPa, 1173 K, $Ba_2Na_3(B_3O_6)_2F$, crystal (b) 3 GPa, 1173 K, $Ba_2Na_3(B_3O_6)_2F$, SPS (c) 3 GPa, 1173 K, $Ba_2Na_3(B_3O_6)_2F$, SPS

(d) 6 GPa, 1173 K, $Ba_2Na_3(B_3O_6)_2F$, crystal (e) 6 GPa, 1173 K, $Ba_2Na_3(B_3O_6)_2F$, SPS (f) 6 GPa, 1173 K, $Ba_2Na_3(B_3O_6)_2F$, crystal

Fig. 8. Backscattered electron images of the products of HPHT experiments at 3 GPa (a–c) and 6 GPa (d–f), 1173 K.

401, 475, 625, 680, 770, 1549, and 1577 cm^{-1} belong to the $NaBO_2$ phase. Correspondingly, an intense peak at 906 cm^{-1}, and less intense peaks at about 181, 203, and 1202 cm^{-1}, which do not coincide with the Raman peaks of the γ-BaB_2O_4 phase [17], might belong to a new high-pressure modification of barium borate, δ-BaB_2O_4. According to a recent numerical study [16–17], γ-BaB_2O_4 should undergo a phase transition at the pressure of about 6 GPa. Further HPHT

Table 2. Compositions of the products of HPHT experiments determined by energy-dispersive X-ray microanalysis

Experimental conditions	Starting mater	Phase	Composition / mol%				
			Ba	B	F	Na	O
3 GPa, 1173 K, 44.5 h	Crystal	$Ba_2Na_3(B_3O_6)_2F$	9.2(1)	23.9(2)	4.1(1)	13.2(1)	49.6(1)
	SPS	$Ba_2Na_3(B_3O_6)_2F$	9.2(1)	23.8(1)	4.2(1)	13.3(1)	49.5(1)
		BaB_2O_4 (trace amount)	16(2)	27(4)	—	—	57(2)
3 GPa, 1173 K, 64 h	Crystal	BaB_2O_4	18(1)	22(1)	—	—	60(2)
		$NaBO_2$	0.9(2)	23.9(2)	0.2(5)	25.5(5)	49.4(3)
		NaF	2.8(3)	4(3)	48(3)	52(4)	10(4)
	SPS	BaB_2O_4	19(2)	21(1)	—	—	60(1)
		$NaBO_2$	0.5(4)	24.2(7)	1(1)	25(1)	49(1)
		NaF	0.9(4)	0.9(2)	47(2)	48.3(1)	3(2)

Note: The numbers in the parentheses represent the standard error in the last digit shown.

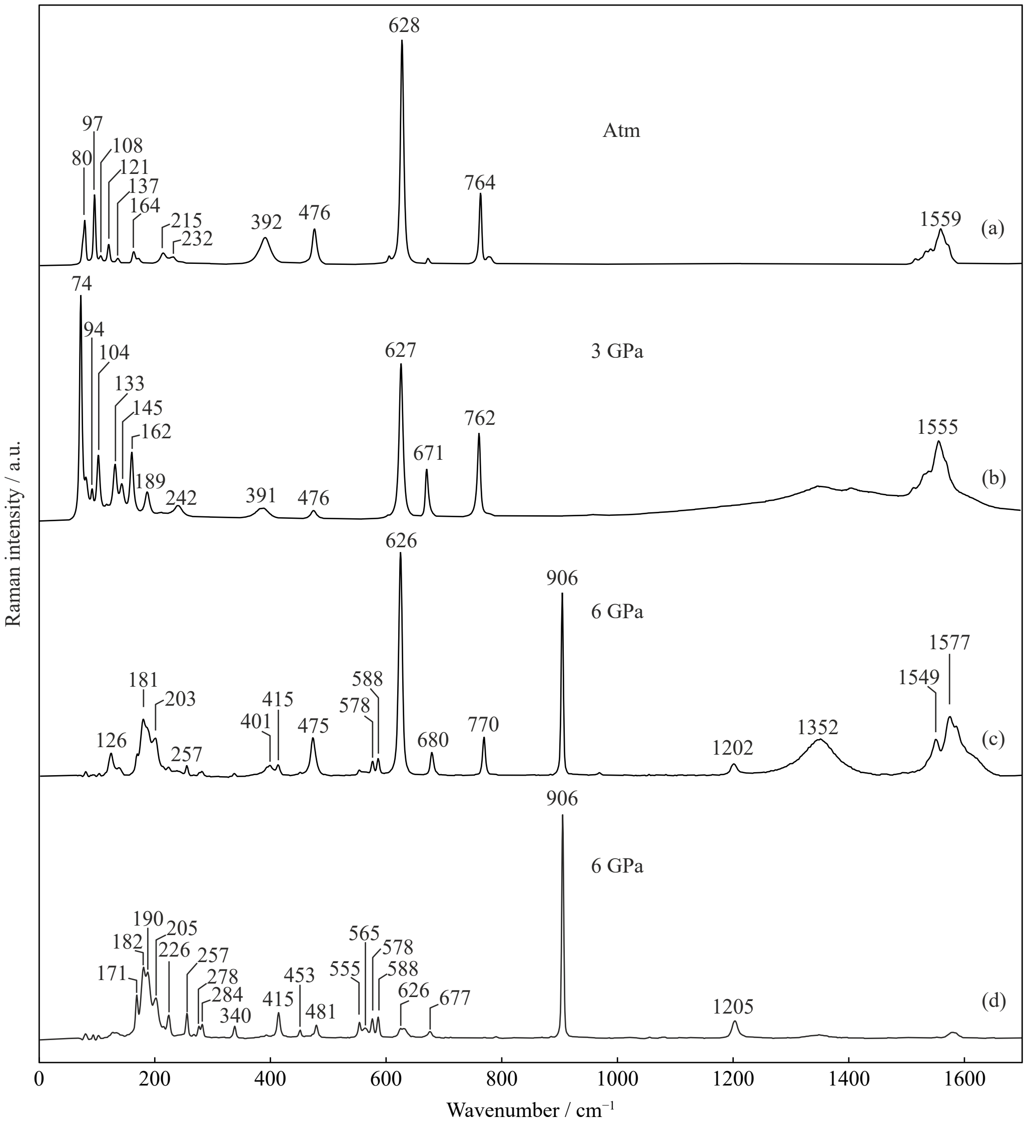

Fig. 9. Raman spectra of $Ba_2Na_3(B_3O_6)_2F$ at (a) atmospheric pressure and (b) 3 GPa; (c,d) reaction products at 6 GPa.

study is needed to obtain δ-BaB_2O_4 crystals large enough for structure refinament.

4. Conclusion

In this work, a high-pressure stability limit of barium–sodium metaborate, $Ba_2Na_3(B_3O_6)_2F$, was studied. Performed DFT calculations showed that $Ba_2Na_3(B_3O_6)_2F$ decompose to $2BaB_2O_4$ + $2NaBO_2$ + NaF at zero temperature above 2.8 GPa without ZPE and 3.1 GPa with ZPE. Phonon calculations suggest that $Ba_2Na_3(B_3O_6)_2F$ could be compressed metastable without heating up to 5 GPa. Taking into account the temperature effect, the *P*–*T* boundary of the decomposition reaction was obtained. In addition, electronic properties were studied. The width of the band gap is 6.289 eV with indirect transition along the Γ–K direction. The main optical transition occurs from O 2*p* to Ba 5*d* levels. Experimental Raman spectrum of $Ba_2Na_3(B_3O_6)_2F$ synthesized at ambient pressure was compared with calculated spectrum which made it possible to attribute the observed modes. The conducted HTHP experiments showed that $Ba_2Na_3(B_3O_6)_2F$ remains stable at 3 GPa, and decomposes to NaF, $NaBO_2$, and BaB_2O_4 at 6 GPa, thereby confirming the correctness of the calculated *P*–*T* diagram. According to the Raman spectra from 6 GPa, there is a new high-pressure modification of BaB_2O_4, named δ-BaB_2O_4. Since the size of δ-BaB_2O_4 crystals does not exceed several microns, it is currently impossible to solve the structure.

Acknowledgements

The SEM and EDX studies of experimental samples were performed in the Analytical Center for Multielemental and Isotope Research SB RAS. This work was financially supported by the Russian Science Foundation (No. 21-19-00097) https://rscf.ru/project/21-19-00097/.

Conflict of Interest

The authors declare that they have no known competing financial interests or personal relationships that could have appeared to influence the work reported in this paper.

Supplementary Information

The online version contains supplementary material available at https://doi.org/10.1007/s12613-023-2647-0

Additional file 1: **Table S1**. Calculated elastic constants C_{ij} of $Ba_2Na_3(B_3O_6)_2F$ at 0, 5, and 10 GPa. **Fig. S1**. Raman spectrum of (a) reaction products at 6 GPa in comparison with (b) Raman spectrum of $NaBO_2$ drawn based on the data of Ref. [42].

Additional file 2: Animated harmonic modes of atom displacements in selected Raman modes of $Ba_2Na_3(B_3O_6)_2F$ at (a) 1559 cm^{-1}, (b) 764 cm^{-1}, (c) 628 cm^{-1}, (d) 476 cm^{-1}, (e) 392 cm^{-1}, (f) 215 cm^{-1}, (g) 121 cm^{-1}, (h) 97 cm^{-1}, and (i) 80 cm^{-1}.

References

[1] T.B. Bekker, A.E. Kokh, N.G. Kononova, P.P. Fedorov, and S.V. Kuznetsov, Crystal growth and phase equilibria in the BaB_2O_4–NaF system, *Cryst. Growth Des.*, 9(2009), No. 9, p. 4060.

[2] X. Wang, M.J. Xia, and R.K. Li, A promising birefringent crystal $Ba_2Na_3(B_3O_6)_2F$, *Opt. Mater.*, 38(2014), p. 6.

[3] H. Zhang, M. Zhang, S.L. Pan, *et al.*, $Na_3Ba_2(B_3O_6)_2F$: Next generation of deep-ultraviolet birefringent materials, *Cryst. Growth Des.*, 15(2015), No. 1, p. 523.

[4] T.B. Bekker, V.N. Vedenyapin, and A.G. Khamoyan, Birefringence of the new fluoride borates $Ba_2Na_3[B_3O_6]_2F$ and $Ba_7(BO_3)_{4-y}F_{2+3y}$ in the Na, Ba, B//O, F quaternary reciprocal system, *Mater. Res. Bull.*, 91(2017), p. 54.

[5] V.D. Antsygin, A.A. Mamrashev, N.A. Nikolaev, O.I. Potaturkin, T.B. Bekker, and V.P. Solntsev, Optical properties of borate crystals in terahertz region, *Opt. Commun.*, 309(2013), p. 333.

[6] M. Marezio, H.A. Plettinger, and W.H. Zachariasen, The bond lengths in the sodium metaborate structure, *Acta Crystallogr.*, 16(1963), No. 7, p. 594.

[7] W. Schneider and G.B. Carpenter, Bond lengths and thermal parameters of potassium metaborate, $K_3B_3O_6$, *Acta Crystallogr. Sect. B*, 26(1970), No. 8, p. 1189.

[8] S. Schmid and W. Schnick, Rubidium metaborate, $Rb_3B_3O_6$, *Acta Crystallogr. C*, 60(2004), No. Pt7, p. i69.

[9] M. Schläger and R. Hoppe, Darstellung und kristallstruktur von $CsBO_2$, *Z. Anorg. Allg. Chem.*, 620(1994), No. 11, p. 1867.

[10] A.D. Mighell, A. Perloff, and S. Block, The crystal structure of the high temperature form of Barium borate, $BaO{\cdot}B_2O_3$, *Acta Crystallogr.*, 20(1966), No. 6, p. 819.

[11] R. Bubnova, S. Volkov, B. Albert, and S. Filatov, Borates—Crystal structures of prospective nonlinear optical materials: High anisotropy of the thermal expansion caused by anharmonic atomic vibrations, *Crystals*, 7(2017), No. 3, art. No. 93.

[12] J. Liebertz, Struktur und kristallchemie von $Ba_2M(B_3O_6)_2$ mit M = Ca, Cd, Mg, Co and Ni, *Z. Kristallogr. Cryst. Mater.*, 168(1984), No. 1-4, p. 293.

[13] G. Sohr, D.M. Többens, J. Schmedt auf der Günne, and H. Huppertz, HP-CsB_5O_8: Synthesis and characterization of an outstanding borate exhibiting the simultaneous linkage of all structural units of borates, *Chem. Eur. J.*, 20(2014), No. 51, p. 17059.

[14] H.F. Dong, A.R. Oganov, V.V. Brazhkin, *et al.*, Boron oxides under pressure: Prediction of the hardest oxides, *Phys. Rev. B*, 98(2018), No. 17, art. No. 174109.

[15] D. Vitzthum, K. Wurst, J.M. Pann, P. Brüggeller, M. Seibald, and H. Huppertz, Exploration into the syntheses of gallium- and indiumborates under extreme conditions: $M_5B_{12}O_{25}(OH)$: Structure, luminescence, and surprising photocatalytic properties, *Angew. Chem. Int. Ed.*, 57(2018), No. 35, p. 11451.

[16] N.E. Sagatov, T.B. Bekker, I.V. Podborodnikov, and K.D. Litasov, First-principles investigation of pressure-induced structural transformations of barium borates in the BaO–B_2O_3–BaF_2 system in the range of 0–10 GPa, *Comput. Mater. Sci.*, 199(2021), art. No. 110735.

[17] T.B. Bekker, I.V. Podborodnikov, N.E. Sagatov, *et al.*, γ-BaB_2O_4: High-pressure high-temperature polymorph of barium borate with edge-sharing BO_4 tetrahedra, *Inorg. Chem.*, 61(2022), No. 4, p. 2340.

[18] H. Huppertz and B. von der Eltz, Multianvil high-pressure synthesis of $Dy_4B_6O_{15}$: The first oxoborate with edge-sharing BO_4 tetrahedra, *J. Am. Chem. Soc.*, 124(2002), No. 32, p. 9376.

[19] G. Kresse and J. Furthmüller, Efficient iterative schemes for *ab initio* total-energy calculations using a plane-wave basis set, *Phys. Rev. B*, 54(1996), No. 16, p. 11169.

[20] G. Kresse and D. Joubert, From ultrasoft pseudopotentials to the projector augmented-wave method, *Phys. Rev. B*, 59(1999), No. 3, p. 1758.

[21] J.P. Perdew, K. Burke, and M. Ernzerhof, Generalized gradient approximation made simple, *Phys. Rev. Lett.*, 77(1996), No. 18, p. 3865.

[22] H.J. Monkhorst and J.D. Pack, Special points for Brillouin-zone integrations, *Phys. Rev. B*, 13(1976), No. 12, p. 5188.

[23] A.V. Krukau, O.A. Vydrov, A.F. Izmaylov, and G.E. Scuseria, Influence of the exchange screening parameter on the performance of screened hybrid functionals, *J. Chem. Phys.*, 125(2006), No. 22, art. No. 224106.

[24] V. Wang, N. Xu, J.C. Liu, G. Tang, and W.T. Geng, VASPKIT: A user-friendly interface facilitating high-throughput comput-

ing and analysis using VASP code, *Comput. Phys. Commun.*, 267(2021), art. No. 108033.

[25] F.W. Aquino, R. Shinde, and B.M. Wong, Fractional occupation numbers and self-interaction correction-scaling methods with the Fermi-Löwdin orbital self-interaction correction approach, *J. Comput. Chem.*, 41(2020), No. 12, p. 1200.

[26] B.G. Janesko, Replacing hybrid density functional theory: Motivation and recent advances, *Chem. Soc. Rev.*, 50(2021), No. 15, p. 8470.

[27] R. Shinde, S.S.R.K.C. Yamijala, and B.M. Wong, Improved band gaps and structural properties from Wannier–Fermi–Löwdin self-interaction corrections for periodic systems, *J. Phys.: Condens. Matter*, 33(2021), No. 11, art. No. 115501.

[28] A. Togo and I. Tanaka, First principles phonon calculations in materials science, *Scr. Mater.*, 108(2015), p. 1.

[29] A. Fonari and S. Stauffer, Vasp_raman.py, 2013 [2016-09-21]. https://github.com/raman-sc.

[30] Q.J. Zheng, VaspVib2XSF, 2020 [2022-11-08]. https://github.com/QijingZheng/VaspVib2XSF.

[31] A. Stukowski, Visualization and analysis of atomistic simulation data with OVITO–the Open Visualization Tool, *Modelling Simul. Mater. Sci. Eng.*, 18(2010), No. 1, art. No. 015012.

[32] J.M. Leger, J. Haines, A. Atouf, O. Schulte, and S. Hull, High-pressure X-ray- and neutron-diffraction studies of BaF_2: An example of a coordination number of 11 in AX_2 compounds, *Phys. Rev. B*, 52(1995), No. 18, p. 13247.

[33] V.T. Deshpande, Thermal expansion of sodium fluoride and sodium bromide, *Acta Crystallogr.*, 14(1961), No. 7, art. No. 794.

[34] S.M. Fang, The crystal structure of sodium metaborate $Na_3(B_3O_6)$, *Z. Kristallogr. Cryst. Mater.*, 99(1938), No. 1-6, p. 1.

[35] F. Mouhat and F.X. Coudert, Necessary and sufficient elastic stability conditions in various crystal systems, *Phys. Rev. B*, 90(2014), No. 22, art. No. 224104.

[36] T.B. Bekker, T.M. Inerbaev, A.P. Yelisseyev, *et al.*, Experimental and *ab initio* studies of intrinsic defects in "antizeolite" borates with a $Ba_{12}(BO_3)_6^{6+}$ framework and their influence on properties, *Inorg. Chem.*, 59(2020), No. 18, p. 13598.

[37] C. Wu, J.L. Song, L.H. Li, M.G. Humphrey, and C. Zhang, Alkali metal-alkaline earth metal borate crystal $LiBa_3(OH)(B_9O_{16})[B(OH)_4]$as a new deep-UV nonlinear optical material, *J. Mater. Chem. C*, 4(2016), No. 35, p. 8189.

[38] A. Jain, S.P. Ong, G. Hautier, *et al.*, Commentary: The materials project: A materials genome approach to accelerating materials innovation, *APL Mater.*, 1(2013), No. 1, art. No. 011002.

[39] S.M. Wan, X.A. Zhang, S.J. Zhao, *et al.*, Growth units and growth habit of α-BaB_2O_4 crystal, *J. Appl. Crystallogr.*, 40(2007), No. 4, p. 725.

[40] X.S. Lv, Y.L. Sun, J. Han, *et al.*, Growth and Raman spectrum of $Ba_2Mg(B_3O_6)_2$ crystal, *J. Cryst. Growth*, 363(2013), p. 220.

[41] P. Ney, M.D. Fontana, A. Maillard, and K. Polgár, Assignment of the Raman lines in single crystal barium metaborate, *J. Phys.: Condens. Matter*, 10(1998), No. 3, p. 673.

[42] Y.K. Voronko, A.A. Sobol, and V.E. Shukshin, Structure of boron–oxygen groups in crystalline, molten, and glassy alkali-metal and alkaline-earth metaborates, *Inorg. Mater.*, 48(2012), No. 7, p. 732.